THE JOURNAL OF PHYSICAL CHEMISTRY B

ARTICLE

pubs.acs.org/JPCB

A Transferable Force Field To Predict Phase Equilibria and Surface Tension of Ethers and Glycol Ethers

Nicolas Ferrando,*[,†,‡] Véronique Lachet,[†] Javier Pérez-Pellitero,[†,§] Allan D. Mackie,[§] Patrice Malfreyt,[⊥] and Anne Boutin[∥]

[†]IFP Energies Nouvelles, 1-4 avenue de Bois-Préau, 92852 Rueil-Malmaison, France

[‡]Laboratoire de Chimie-Physique, CNRS, Université Paris-Sud, bât. 349, 91405 Orsay Cedex, France

[§]Departament d'Enginyeria Química, ETSEQ, Universitat Rovira i Virgili, Avinguda dels Països Catalans, 26 Campus Sescelades, 43007 Tarragona, Spain

[⊥]Clermont Université, Université Blaise Pascal, Laboratoire de Thermodynamique et Interactions Moléculaires, UMR CNRS 6272, BP 10448, F-63000, Clermont-Ferrand, France

[∥]Ecole Normale Supérieure, Département de Chimie, UMR 8640, CNRS-ENS-UPMC, 24, rue Lhomond, 75005 Paris, France

Supporting Information

ABSTRACT: We propose a new transferable force field to simulate phase equilibrium and interfacial properties of systems involving ethers and glycol ethers. On the basis of the anisotropic united-atom force field, only one new group is introduced: the ether oxygen atom. The optimized Lennard−Jones (LJ) parameters of this atom are identical whatever the molecule simulated (linear ether, branched ether, cyclic ether, aromatic ether, diether, or glycol ether). Accurate predictions are achieved for pure compound saturated properties, critical properties, and surface tensions of the liquid−vapor interface, as well as for pressure−composition binary mixture diagrams. Multifunctional molecules (1,2-dimethoxyethane, 2-methoxyethanol, diethylene glycol) have also been studied using a recently proposed methodology for the calculation of the intramolecular electrostatic energy avoiding the use of additional empirical parameters. This new force field appears transferable for a wide variety of molecules and properties. It is furthermore worth noticing that binary mixtures have been simulated without introducing empirical binary parameters, highlighting also the transferability to mixtures. Hence, this new force field gives future opportunities to simulate complex systems of industrial interest involving molecules with ether functions.

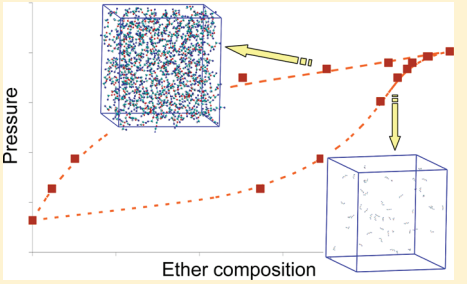

1. INTRODUCTION

Because of their various applications as solvents in biochemistry and organic chemistry, there is considerable interest in the thermophysical properties of ethers. Aliphatic and cyclic ethers are used as solvents or cosolvents in chromatographic stationary phases, organic synthesis, and supercritical fluids. Ethers are also involved in a large variety of industrial processes in the oil and gas industry. Cyclic ethers such as tetrahydrofuran (THF) are particularly suitable for hydrate-based gas separations since they can be added to promote clathrate hydrate formation.[1] Multifunctional ethers such as glycol ethers are involved in gas sweetening and dehydration processes.[2,3] The production of biofuels by incorporating aliphatic ethers to classical fuels, such as dimethyl ether in liquefied petroleum[4] or diethyl ether in diesel,[5] is also of primary interest nowadays. All of these applications require a good knowledge of phase equilibrium and phase properties of both pure fluids and mixtures involving this class of oxygenated compounds. Reliable and predictive models are thus needed in this context.

In the last few years, transferable united-atom force fields have been developed to make molecular simulation an efficient tool to predict equilibrium properties of pure fluids and mixtures with an acceptable precision and a reduced computational time.[6] However, transferable united-atom force fields for ethers are relatively scarce in literature. The OPLS-UA force field (Optimized Potential for Liquid Simulations) developed by Briggs et al. for dimethyl, ethyl methyl, and diethyl ether was proposed to reproduce thermodynamic quantities near room temperature and pressure.[7] Far away from these conditions, this model becomes less accurate, and the transferability to other ethers is questionable. To account for a better and more general description, Stubbs et al. proposed an extension of the TraPPE-UA force field (TRAnsferable Potentials for Phase Equilibria) based on the development of parameters for the ether oxygen atom combined with previously optimized parameters for the rest of the molecule.[8] The simulation of glycol ether molecules is however restrained to the use of a specific intramolecular repulsion potential making this approach less transferable for multifunctional molecules.

Received: April 8, 2011
Revised: July 28, 2011
Published: July 29, 2011

Table 1. Non-bonded Parameters for the AUA4 Force Field

atom	ε (K)	σ (Å)	δ (Å)	q (e)
CH_3 ($-CH_x$)	120.15	3.607	0.216	0
CH_3 ($-O_{ether}$)	120.15	3.607	0.216	+0.223 (dimethyl ether and multifunctional ethers); +0.185 (linear and branched monoethers)
(CH_x-)$CH_{2linear}$ ($-CH_x$)	86.29	3.461	0.384	0
(CH_x-)$CH_{2linear}$ ($-O_{ether}$)	86.29	3.461	0.384	+0.223 (dimethyl ether and multifunctional ethers); +0.185 (linear and branched monoethers)
(CH_x-)$CH_{2linear}$ ($-O_{alcohol}$)	86.29	3.461	0.384	+0.265
($CH_{2cyc}-$)CH_{2cyc}($-CH_{2cyc}$)	90.09	3.461	0.336	0
($CH_{2cyc}-$)CH_{2cyc}($-O_{ether}$)	90.09	3.461	0.336	+0.295
(CH_x-)CH_{aliph}($-O_{ether}$)	50.98	3.363	0.646	+0.185
(CH_x-)C_{aliph}($-O_{ether}$)	15.04	2.44	0	+0.185
CH_{arom}	89.40	3.246	0.407	0
C_{arom}($-O_{ether}$)	37.70	3.246	0	+0.223
$O_{alcohol}$	125.01	3.081	0.01	−0.700
$H_{alcohol}$	0	0	0	+0.435
O_{ether}	59.69	2.991	0	−0.446 (dimethyl ether, aromatic ethers, and multifunctional ethers); −0.370 (linear and branched monoethers); −0.590 (cyclic ethers)

In this work, we propose to extend the transferable AUA4 potential[9] to ethers by introducing a single new atom corresponding to the ether oxygen. For the shake of transferability, all of the other groups are taken from previous parametrizations of the AUA4 force field (see ref 6 for a review), and the new Lennard−Jones (LJ) parameters of the oxygen force center proposed in this work are the same whatever the ether simulated. To highlight the transferability of the developed force field, various families of ethers are studied (linear, branched, cyclic, aromatic, diethers, and glycol ethers). At the same time, binary mixtures with hydrocarbons and alcohols are considered. In addition to the prediction of classical saturated phase properties, we also calculate the liquid−vapor surface tension of dimethyl ether using the new force field.

This paper is organized as follows: the proposed force field is described in Section 2. The simulation methods used to calculate phase equilibrium and interfacial properties of pure compounds and binary mixtures are detailed in Section 3. Section 4 presents the results obtained for saturated properties, liquid phase structure, and surface tension predictions of a wide variety of pure ethers as well as phase diagrams of mixtures. Finally, Section 5 gives our conclusions.

2. FORCE FIELD DEVELOPMENT

2.1. Intermolecular Energy. *2.1.1. Dispersive-Repulsive Energy.* The dispersive-repulsive intermolecular interactions between two force centers i and j are described through a 12-6 LJ potential:

$$U_{ij}^{LJ} = 4\varepsilon_{ij}\left[\left(\frac{\sigma_{ij}}{r_{ij}}\right)^{12} - \left(\frac{\sigma_{ij}}{r_{ij}}\right)^{6}\right] \quad (1)$$

where r_{ij}, ε_{ij}, and σ_{ij} are the distance, the LJ well depth, and the LJ size, respectively.

Cross LJ parameters are obtained using Lorentz−Berthelot combining rules:

$$\varepsilon_{ij} = \sqrt{\varepsilon_{ii}\varepsilon_{jj}} \quad (2)$$

$$\sigma_{ij} = \frac{1}{2}(\sigma_{ii} + \sigma_{jj}) \quad (3)$$

All of the LJ parameters involved in the hydrocarbonated and hydroxyl parts of the molecules studied in this work are taken without any modification from the AUA4 potential for hydrocarbons[9−12] and alcohols.[13] The totality of the parameters are summarized in Table 1. In the AUA model, the LJ center is not located on the atomic nuclei of the group but slightly shifted by a distance δ (AUA displacement) to implicitly take into account the presence of its bonded hydrogen atoms. In this work, a single new force center is introduced for the ether oxygen atom. Since no AUA displacement is required in the case of this center of force, the only parameters to be adjusted are the LJ parameters σ_0 and ε_0.

The optimization procedure applied for the LJ parameters used in this work has been described elsewhere.[14] It consists in minimizing the mean square relative deviation F between experimental and calculated properties X_i:

$$F = \frac{1}{n}\sum_{i=1}^{n}\frac{(X_i^{calc} - X_i^{exp})^2}{s_i^2} \quad (4)$$

where n denotes the total number of target values and s the sum of statistical and experimental uncertainties for a given property. The properties used in this adjustment procedure are the saturated liquid density, vapor pressure, and vaporization enthalpy of ethyl methyl ether at temperatures of 280 and 420 K. The experimental associated uncertainties are 1.5%, 5%, and 2%, respectively. This compound has been selected due to the fact that it includes both CH_2 and CH_3 neighboring ether group effects. The final optimized LJ parameters are given in Table 1.

dx.doi.org/10.1021/jp203278t |J. Phys. Chem. B 2011, 115, 10654–10664

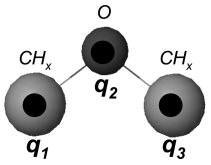

Figure 1. Schematic representation of the ether function in the proposed molecular model. q_1, q_2, and q_3 stand for the partial electrostatic charges located on the carbon and oxygen atoms.

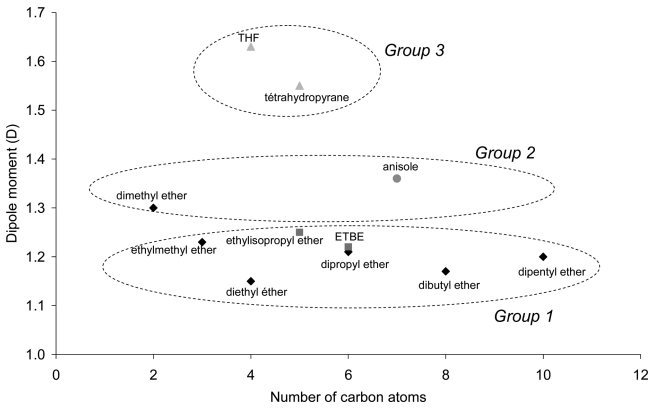

Figure 2. Experimental[15] gas phase dipole moments of ethers (diamonds: linear ethers, squares: branched ethers, circles: aromatic ethers, triangles: cyclic ethers).

2.1.2. Electrostatic Energy. The electrostatic interaction between two partial electrostatic charges i and j is modeled by the Coulomb potential:

$$U_{ij}^{\text{elec}} = \frac{q_i q_j}{4\pi\varepsilon_0 r_{ij}} \tag{5}$$

where r_{ij} is the distance between charges i and j, q_i the magnitude of charge i, and ε_0 the vacuum permittivity.

We adopt a three partial charge distribution involving one negative charge located on the oxygen atom and two symmetric positive charges on the bonded carbonated groups (see illustration in Figure 1). Concerning the magnitude of these charges, the use of a unique set of charges for the totality of the studied ether molecules is questionable. The transferability of electrostatic charges is justified as long as all studied molecules have a similar dipole moment. Figure 2 shows the evolution of the experimental gas phase dipole moment of various linear, branched, cyclic and aromatic ethers in function of the number of carbon atoms.[15] In light of this graph, we propose to split the molecules in three groups. The first group (denoted further as group 1) contains branched and linear ethers (except dimethyl ether). The second group (group 2) contains dimethyl ether and aromatic ethers, and finally the third group (group 3) is constituted by cyclic ethers. Consequently, three different sets of partial electrostatic charges are proposed. It is well-known that the dipole moment of a polarizable molecule significantly differs between the gas phase and the liquid phase, and it is widely admitted that molecular models yield better results for phase equilibrium prediction when using the liquid phase dipole moment.[16] Hence, to determine the magnitude of the three sets of charges, we adopt a procedure similar to that described by Eckl et al.:[17,18] an ab initio calculation is performed by placing a molecule in a dielectric medium whose

Table 2. Bonded Parameters for the AUA4 Force Field

bond length		r_0 (Å)
CH_x—CH_y		1.535
CH_x—$O_{ether/alcohol}$		1.43
C_{arom}—O_{ether}		1.36
C_{arom}=C_{arom}		1.40
$O_{alcohol}$—H		0.945
bend	θ_0 (deg)	k_{bend} (K)
CH_x—CH_2—CH_y	114.0	74900
CH_x—CH_2—$O_{ether/alcohol}$	109.47	59800
CH_x—CH —O_{ether}	112.0	57500
CH_x—C—O_{ether}	112.0	57500
CH_x—O_{ether}—CH_y	112.0	69000
CH_{arom}=CH_{arom}=CH_{arom}	120.0	rigid
CH_{arom}=C_{arom}—$O_{ether/alcohol}$	120.0	rigid
C_{arom}—O_{ether}—CH_x	112.0	69000
CH_x—$O_{alcohol}$—H	108.5	61000
torsion	a_i (K)	
CH_x—CH_2—CH_2—CH_y	a_0 = 1001.35	a_1 = 2129.52
	a_2 = −303.06	a_3 = −3612.27
	a_4 = 2226.71	a_5 = 1965.93
	a_6 = −4489.34	a_7 = −1736.22
	a_8 = 2817.37	
CH_x—CH_2—CH_2—O_{ether}	a_0 = 839.87	a_1 = 2133.17
	a_2 = 106.68	a_3 = −3079.72
CH_x—CH_2—CH_2—$O_{alcohol}$	a_0 = 839.87	a_1 = 2133.17
	a_2 = 106.68	a_3 = −3079.72
CH_x—CH_2—O_{ether}—CH_y	a_0 = 956.05	a_1 = 949.25
	a_2 = 327.50	a_3 = −2232.80
CH_x—CH_2—O_{ether}—C_{arom}	a_0 = 956.05	a_1 = 949.25
	a_2 = 327.50	a_3 = −2232.80
CH_3—CH—O_{ether}—CH_y	a_0 = 373.05	a_1 = 919.04
	a_2 = 268.15	a_3 = −1737.21
CH_3—C—O_{ether}—CH_y	a_0 = 230.65	a_1 = 691.92
	a_2 = 0	a_3 = −922.58
CH_{arom}=CH_{arom}=CH_{arom}=CH_{arom}	rigid	
CH_{arom}=CH_{arom}=C_{arom}—$O_{ether/alcohol}$	rigid	
$O_{alcohol}$=C_{arom}=C_{arom}—O_{ether}	rigid	
C_{arom}=C_{arom}—$O_{alcohol}$—H	a_0 = 845.65	a_1 = 0
	a_2 = −845.65	a_3 = 0
CH_{arom}=C_{arom}—O_{ether}—CH_x	a_0 = 1631.27	a_1 = 2651.77
	a_2 = 868.86	a_3 = −2184.14
	a_4 = −3028.37	a_5 = −3065.12
	a_6 = 1926.79	a_7 = 1723.03
	a_8 = −497.96	
O_{ether}—CH_2—CH_2—O_{ether}	a_0 = 586.06	a_1 = 2775.61
	a_2 = 2496.45	a_3 = −2542.12
	a_4 = −3132.43	a_5 = −2249.38
	a_6 = 4188.47	a_7 = 1318.58
	a_8 = −2316.03	
CH_2—CH_2—$O_{alcohol}$—H	a_0 = 339.41	a_1 = 353.97
	a_2 = 58.34	a_3 = −751.72
O_{ether}—CH_2—CH_2—$O_{alcohol}$	a_0 = 1530.22	a_1 = 4064.26
	a_2 = −422.78	a_3 = −5570.19

Table 2. Continued

torsion	a_i (K)
$a_4 = -772.20$	$a_5 = 1110.27$
$a_6 = 174.93$	$a_7 = 430.66$
$a_8 = 534.83$	

dielectric constant is equal to that of the neat liquid of the given molecule, and the magnitude of the partial charges are adjusted to reproduce the obtained dipole moment. Preliminary ab initio calculations using the Jaguar software (v.7.0, Schrödinger LLC, 2007) have shown that the B3LYP/6-311G** level of theory gives an accurate prediction of experimental gas phase dipole moments (see Figure S1 in the Supporting Information). Hence, this level of theory is used for the calculation in the dielectric medium. Three calculations are performed: the first one with a molecule of diethyl ether (dielectric constant of 4.27) for the determination of group 1 charges, the second one with a molecule of dimethyl ether (dielectric constant of 6.18) for group 2 charges, and the third one with a molecule of THF (tetrahydrofuran, dielectric constant of 7.52) for group 3 charges. The resulting liquid phase dipole moments are 1.43 D, 1.69 D, and 2.32 D, respectively, which corresponds to increases from 25 to 40% compared to their respective experimental gas phase dipole moments. The resulting electrostatic charges are reported in Table 1.

To simulate oxygenated multifunctional molecules involving an ether function (1,2-dimethoxyethane, 2-methoxyethanol, diethylene glycol), we take advantage of the transferability of the force field and directly use the LJ parameters and partial charges of monoethers without any readjustment. The choice of the set of electrostatic charges to be used (group 1 or group 2) is not evident in some cases. To determine which set of charges is the most appropriate, ab initio calculations in a dielectric medium have been carried out to determine the liquid phase dipole moment of 1,2-dimethoxyethane (dielectric constant of 7.3), 2-methoxyethanol (dielectric constant of 16.98), and diethylene glycol (dielectric constant of 31.82) in their most stable conformations. Then, the dipole moments are calculated using both sets of charges and compared to the ab initio value. Results are detailed in Supporting Information (Table S1) and show that the group 2 set of charges yields a better restitution of the ab initio liquid phase dipole moment. This set of charges will be thus systematically used to model multifunctional molecules.

2.2. Intramolecular Energy. All of the bonded parameters involved in the intramolecular energy calculation are given in Table 2. In the proposed force field, all bond lengths are kept fixed. The CH_x—O_{ether} bond length is chosen equal to the CH_x—$O_{alcohol}$ bond length used in the parametrization of the force field for alcohols.[13] The C_{arom}—O_{ether} bond length encountered in anisole is taken from Lide.[19] The rest of bond lengths are taken from the AUA4 force field.[6] Atoms separated by two bonds interact via a harmonic bending potential:

$$\frac{U_{bend}}{k_B} = \frac{1}{2} k_{bend}(\cos\theta - \cos\theta_0)^2 \qquad (6)$$

where k_B is the Boltzmann constant, k_{bend} the bending constant, and θ and θ_0 the bending angle and the equilibrium bending angle, respectively. The bending parameters involving the ether oxygen atom are taken from the AMBER force field,[20] whereas all other bending parameters are taken from the AUA4 force field.

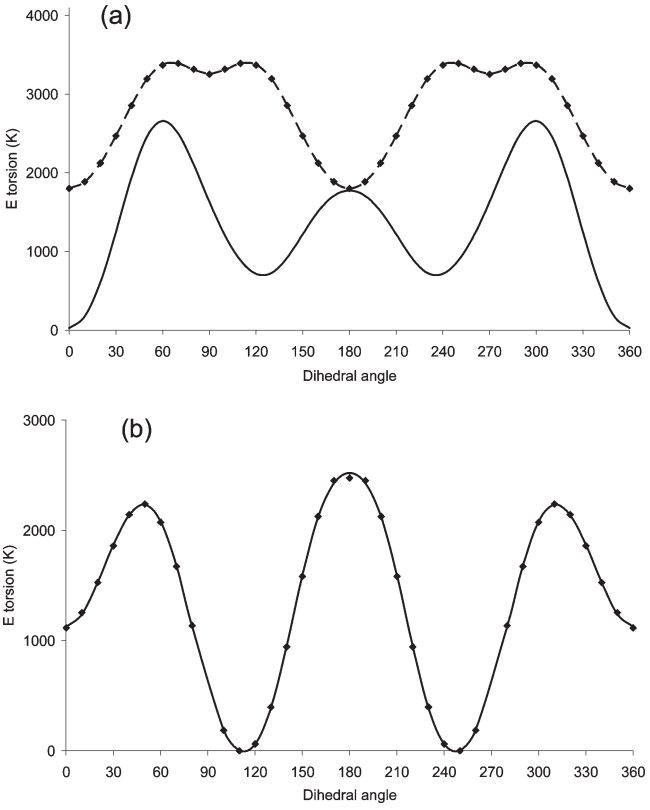

Figure 3. Torsion energy as a function of the dihedral angle. The convention used is that a dihedral angle equal to 0 corresponds to a *trans* conformation. Symbols denote data derived from ab initio calculations, while solid lines are the corresponding fittings to eq 7. (a) CH_{arom}═C_{arom}—O_{ether}—CH_3 in anisole (ab initio data correspond to the sum of the two torsions of this type encountered in anisole assuming a shift of 180° between the two dihedral angles; the dashed line corresponds to the fit of the sum of the two torsions). (b) O_{ether}—CH_2—CH_2—O_{ether} in 1,2-dimethoxyethane.

For atoms separated by three bonds, a torsion potential of the following form is used:

$$\frac{U_{tors}}{k_B} = \sum_{n=0}^{8} a_n(\cos\varphi)^n \qquad (7)$$

where φ is the dihedral angle and a_i the ith torsion parameter. If available, the torsion parameters are taken from the OPLS-UA force field.[7] The missing torsions CH_3—CH—O_{ether}—CH_x and CH_3—C—O_{ether}—CH_x encountered in ethylisopropyl ether and in ETBE (ethyl *tert*-butyl ether) are assumed to be identical to the AUA4 CH_3—CH—CH_2—CH_x and CH_3—C—CH_2—CH_x torsions, respectively.[10,21] The O_{ether}—CH_2—CH_2—$O_{alcohol}$ torsion is assumed identical to the $O_{alcohol}$—CH_2—CH_2—$O_{alcohol}$ torsion encountered in 1,2-ethanediol.[13] The CH_{arom}═C_{arom}—O_{ether}—CH_x torsion encountered in anisole is determined as follows. Ab initio calculations have been carried out on an isolated anisole molecule using the Jaguar software (v.7.0, Schrödinger LLC, 2007), with the MP2 method and 6-311G** basis set. The energy was obtained for the whole range of the CH_{arom}═C_{arom}—O_{ether}—CH_3 torsion angle, from 0 to 360°, with increments of 10°. For each configuration, the contribution of bending and intramolecular LJ energies are subtracted from the total ab initio energy. Thus, the resulting

energy corresponds to the missing torsion potential, and it is fitted according to eq 7. Finally, the $O_{ether}—CH_2—CH_2—O_{ether}$ torsion encountered in 1,2-dimethoxyethane is determined from quantum calculations in the same manner. The torsion potentials determined in this work are plotted in Figure 3.

For the multifunctional molecules studied in this work, intramolecular electrostatic energy is taken into account following a previously described methodology employed for polyhydric alcohols.[13] The Coulomb law is applied between electrostatic charges belonging to the different local dipoles of the molecule, even if charges are located on bonded atoms (note that the torsion potential determinations are carried out in accordance with this methodology). The description of the existing local dipoles of the studied molecules is given in the Supporting Information (Figure S2).

Finally, a 12-6 LJ potential is used to calculate repulsive—dispersive intramolecular energy between two force centers separated by more than three bonds with identical parameters to those used for intermolecular interactions. As already pointed out in a previous work,[13] it is also necessary to apply this contribution between an hydroxyl oxygen atom and any other oxygen atom separated by exactly three bonds (in this work, it is the case for 2-methoxyethanol and diethylene glycol for which 1−4 oxygen−oxygen interaction exits), to avoid a too-strong attraction between the hydroxyl hydrogen atom, not surrounded by a LJ sphere, and the other oxygen atom.

3. SIMULATION METHODS

3.1. Phase Equilibria. All of the bulk liquid−vapor equilibrium simulations of pure compounds were carried out in the NVT Gibbs ensemble.[22,23] In this ensemble, the two phases in equilibrium are introduced in two separate boxes without an explicit interface. When employed to study pure component equilibrium, this ensemble is applied at constant total volume of the two phases to respect the phase rule, the temperature and the total number of molecules being also imposed. A total number of 300 molecules was used for each system, except in the vicinity of the critical point where larger systems were used (up to 500 molecules). For monofunctional ethers and 1,2-dimethoxyethane, the simulation runs lasted for 50 million steps (involving an equilibration run of 25 million steps), one step corresponding to a single Monte Carlo (MC) move. The simulations of glycol ethers require longer equilibrium runs, and the statistical fluctuations observed are slightly more important, requiring thus also longer production runs to reduce statistical uncertainties. Hence, the simulation runs for glycol ethers lasted for 80 million steps involving an equilibration run of 40 million steps. In the case of LJ interactions, a spherical cutoff equal to half of the simulation box was used while the classical tail correction was employed.[24] For long-range electrostatic energy, the Ewald summation technique was used, with a number of reciprocal vectors k equal to 7 in all three space directions and a Gaussian width α^{red} equal to 2 in reduced units. This reduced parameter is related to the α parameter with:

$$\alpha = \alpha^{red}\pi/L \tag{8}$$

where L is the simulation box length.

The different Monte Carlo moves and their correspondent attempt probabilities used during the simulations depend on the studied molecule and are summarized in the Supporting Information (Table S2). Note that the regrowth move is performed using the configurational bias.[25] For cyclic aliphatic molecules, the transfer moves involve a specific reservoir bias[11] which allows us to sample the different conformations of the cycle. A high attempt probability is imposed for this transfer move since its acceptation ratio is low (0.5% at low reduced temperatures to 2% at high reduced temperatures). The amplitude of translations, rigid rotations, and volume changes was adjusted during the simulation to achieve an acceptance ratio of 40% for these moves.

The critical properties T_C and ρ_C of pure compounds were estimated by a least-squares fit of the law of rectilinear diameters:

$$\frac{\rho_l + \rho_v}{2} = \rho_C + A(T - T_C) \tag{9}$$

where ρ_l and ρ_v are the density of the liquid and vapor phases, respectively, T the temperature, and A an adjustable parameter, and the critical scaling relation:

$$\rho_l - \rho_v = B(T - T_C)^{\beta} \tag{10}$$

where B is another adjustable parameter and β the universal exponent, equal to 0.325.[25] This procedure works well for nonpolar molecules, but it has also been successfully applied for the prediction of the critical properties of polar molecules such as alcohols, ketones, and aldehydes.[13,26] Finally, the normal boiling temperatures of the pure compounds were determined using the Clausius−Clapeyron equation. Note that vapor pressure is calculated using the virial equation in the vapor phase and the molar vaporization enthalpy h^{vap} with the following relationship:

$$h^{vap} = N_a\left(\frac{\langle U^{vap}\rangle}{\langle N^{vap}\rangle} - \frac{\langle U^{liq}\rangle}{\langle N^{liq}\rangle} + P^{vap}\left(\frac{\langle V^{vap}\rangle}{\langle N^{vap}\rangle} - \frac{\langle V^{liq}\rangle}{\langle N^{liq}\rangle}\right)\right) \tag{11}$$

where N_a is the Avogadro number, P^{vap} the pressure calculated in the vapor phase, and $\langle U^i\rangle$, $\langle N^i\rangle$, and $\langle V^i\rangle$ the average potential energy, total number of molecules, and volume of phase i, respectively.

For the binary mixtures studied in this work, simulations are performed in the bubble point pseudoensemble using the so-called hybrid method.[27,28] This methodology has already been successfully applied for nonpolar and polar mixtures with a good efficiency.[26,28,29] The liquid phase composition is kept fixed during the simulation, while pressure and vapor composition are given as results from the calculation. In the hybrid method, a first simulation in the bubble-point pseudoensemble (BPMC) is carried out, and then the obtained results are used to initialize a simulation in the isotherm-isochore Gibbs ensemble (GE-NVT) with the main goal of reducing the statistical uncertainty in the pressure calculation. Both BPMC and GE-NVT simulations lasted for 50 to 80 million MC steps, including an equilibrium run of 30 million steps. The initial number of molecules in the liquid phase was 400. All other simulation parameters are similar to those previously described for pure component systems.

3.2. Surface Tension. To check the accuracy of the developed force field to predict interfacial properties, the surface tension γ of dimethyl ether has been calculated. The simulations have been carried out in the NVT ensemble in a rectangular parallelepipedic box. We have considered a system with two planar liquid−vapor surfaces lying in the x,y-plane and the z-axis in the direction

normal to the surface (see Figure S5 in the Supporting Information). As the geometry of the system shows a heterogeneity along the axis normal to the interface (z-axis), we calculated the long-range correction to the repulsion-dispersion energy as a function of z_k by splitting the cell into slabs. The total long-range correction energy U_{LRC} was then calculated by summing up all of the local contributions of each slab. The U_{LRC} term was then added in the total energy of the system to be used in the Metropolis scheme. This long-range correction to the LJ energy is defined by two parts:[30]

$$U_{LRC} = \sum_{i=1}^{N_s} u_{lrc}(z_k) = \sum_{i=1}^{N_s} (u_{lrc}^{(1)}(z_k) + u_{lrc}^{(2)}(z_k)) \quad (12)$$

where N_s is the total number of slabs in the simulation box and with:

$$u_{lrc}^{(1)}(z_k) = \frac{8\pi}{3}\rho(z_k)^2 V_S \sum_{a=1}^{N_i}\sum_{b=1}^{N_j} \varepsilon_{ab}\left[1/3\left(\frac{\sigma_{ab}^{12}}{r_c^9}\right) - \left(\frac{\sigma_{ab}^{6}}{r_c^3}\right)\right] \quad (13)$$

$$u_{lrc}^{(2)}(z_k) = \pi\rho(z_k)V_S\int_{r_c}^{\infty} dr \int_{-r}^{r} d\Delta z \sum_{i=1}^{N_s}[\rho(z_i) - \rho(z_{i-1})]rU_{LJ,m}(r) \quad (14)$$

where N_s is the now the number of slabs between z and z_k, $\rho(z_k)$ is the density of the slab k, and V_S the volume of the slab. N_i is the number of force centers in molecule i, and $U_{LJ,m}$ is the intermolecular LJ energy with r being the distance between two centers of mass of molecules i and j. It has been shown[31] that the second part of the long-range energy $u_{lrc}^{(2)}$ represents only a minor contribution to the total long-range energy. Therefore, it has not been considered in this work.

Two different methods have been used to calculate surface tensions. The first one is the Irving−Kirkwood (IK) method[32] based on the mechanical definition of the surface tension and requiring the calculation of the local tangential p_T and normal p_N components of the pressure tensor:

$$\gamma_{IK} = \frac{1}{2}\int_{-L_z/2}^{L_z/2}[p_N(z) - p_T(z)]dz \quad (15)$$

where L_z is the length of the simulation box along the z-axis. The components of the pressure tensor in the IK definition are expressed by:

$$p_{\alpha\beta}(z_k) = \langle\rho(z_k)\rangle k_B T\mathbf{I} + \frac{1}{A} \times\left\langle\sum_{i=1}^{N-1}\sum_{j>i}^{N}(r_{ij})_\alpha(F_{ij})_\beta\frac{1}{|z_{ij}|}\theta\left(\frac{z_k - z_i}{z_{ij}}\right)\theta\left(\frac{z_j - z_k}{z_{ij}}\right)\right\rangle \quad (16)$$

where $\mathbf{I}$ is the unit tensor and T the input temperature. α and β represent x, y, or z directions. $\theta(z)$ is the unit step function defined by $\theta(x) = 0$ when $x < 0$ and $\theta(x) = 1$ when $x \geq 0$. A is the surface area normal to the z-axis. The distance z_{ij} between two molecular centers of mass is divided into N_s slabs of thickness δz. Following Irving and Kirkwood, the molecules i and j give a local contribution to the pressure tensor in a given slab k if the line joining the centers of mass of molecules i and j crosses, starts, or finishes in the slab k. Each slab has $1/N_s$ of the total contribution from the $i-j$ interaction. The normal component $p_N(z_k)$ is equal to $p_{zz}(z_k)$, whereas the tangential component is given by $1/2(p_{xx}(z_k) + p_{yy}(z_k))$. $\langle\rho(z_k)\rangle$ is the average density of the slab k. F_{ij} is the intermolecular force between molecules i and j and is expressed as the sum of all of the site−site forces acting between these two molecules.

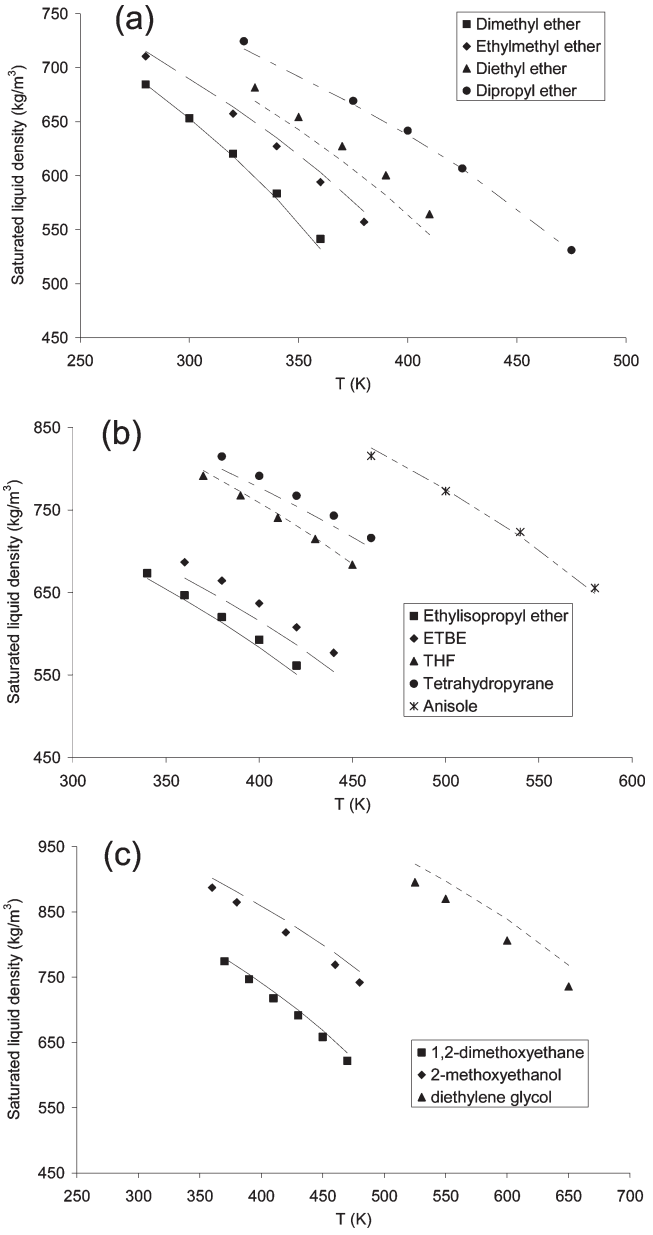

Figure 4. Experimental[15] (lines) and calculated (symbols) saturated liquid densities of linear ethers (a), branched, cyclic, and aromatic ethers (b), and multifunctional ethers (c).

The second method used is the test-area (TA) method,[33] based upon a thermodynamic route and expressing the surface tension as a change in the free energy F for a change in the surface area. This change in the area is performed through a perturbation process for which the perturbed system (state $A + \Delta A$) is obtained from a change ΔA of the area A of the reference system. The box dimension ($L_x^{A+\Delta A}$, $L_y^{A+\Delta A}$, $L_z^{A+\Delta A}$) in the perturbed systems are changed using the following transformations:

dx.doi.org/10.1021/jp203278t |J. Phys. Chem. B 2011, 115, 10654–10664

$L_x^{A+\Delta A} = L_x^A(1+\xi)^{1/2}$, $L_y^{A+\Delta A} = L_y^A(1+\xi)^{1/2}$, and $L_z^{A+\Delta A} = L_z^A/(1+\xi)$ where $\xi \rightarrow 0$. The area $(A + \Delta A)$ of the perturbed state thus equals $L_x^A L_y^A(1+\xi)$, and ΔA is equal to $L_x^A L_y^A \xi$. These transformations conserve the volume of the box in the perturbed state. In this method, several simulations should in principle be repeated for different ξ values to correctly extrapolate the surface tension for ξ approaching zero. However, as recommended by Biscay et al.[34,35] we have performed one simulation with a ξ parameter equals to 5×10^{-4} since it has been shown to give correct surface tension. The operational expression for the calculation of γ within the TA method is:

$$\gamma_{TA} = \left(\frac{\partial F}{\partial A}\right)_{N,V,T} = \sum_k \lim_{\xi \rightarrow 0} -\frac{k_B T}{\Delta A} \ln\left\langle \exp\left(-\frac{(U^{(A+\Delta A)}(z_k, \mathbf{r}'^N) - U^{(A)}(z_k, r^N))}{k_B T}\right)\right\rangle_{k,A} \quad (17)$$

$\langle ... \rangle_{k,A}$ indicates that the average is carried out over the reference state and the k slabs. $U^{(A+\Delta A)}(z_k, \mathbf{r}'^N)$ and $U^{(A)}(z_k, \mathbf{r}^N)$ are the configurational energies of the slab k in the perturbed and reference state.

Tail corrections to the surface tension have also been accounted for using the expressions given by Biscay et al.[36] More detailed descriptions of these models and long-range corrections to be applied can be found elsewhere[31,37−42] and will be not discussed in this work. Note that both methods have been successfully applied with the AUA4 force field to calculate surface tensions of various hydrocarbons.[34,43]

The initial configuration of the system was prepared from equilibrated bulk liquid and bulk vapor phases, the bulk liquid phase (containing 750 molecules) being surrounded by two bulk vapor phases (containing each of them 10 molecules) along the z-axis. The L_x and L_y dimensions of the resulting simulation box are fixed to 30 Å, and the L_z dimension varies from 260 to 420 Å according to the temperature. The Ewald sum technique is used to calculate electrostatic energy, with a number of reciprocal vectors equal to 8 along the x- and y-axis and equal to $(8L_z)/L_x$ along the z-axis. The Monte Carlo moves and their attempt probabilities used during the simulations are: translation (33.5%), rigid rotation (33.5%), and configurational-bias regrowth (33%). A typical simulation consists of an equilibration run followed by a production run of around 320 and 170 million steps, respectively.

4. RESULTS

4.1. Phase Equilibria. *4.1.1. Pure Compounds.* Figures 4, 5, and 6 show respectively a comparison between experimental[15] and calculated saturated liquid densities, vapor pressures, and vaporization enthalpies. For each case different families of ethers are considered: linear ethers (dimethyl ether, ethylmethyl ether, diethyl ether, dipropyl ether), branched ethers (ethylisopropyl ether, ethyltertiobutyl ether (ETBE)), cyclic ethers (THF, tetrahydropyrane), aromatic ether (anisole), diether (1,2-dimethoxyethane), and glycol ethers (2-methoxyethanol, diethylene glycol). Numerical values are provided in the Supporting Information (Table S3). The properties of monofunctional ethers are predicted with a good accuracy. Average deviations between calculated and experimental saturated liquid densities, vapor pressures, and vaporization enthalpies are 1.5%, 8%, and 3%, respectively. These deviations are of the same order of magnitude as those obtained for their corresponding hydrocarbons with the AUA4 force field. The most important deviations are observed for the prediction of THF vapor pressures (23%). Similar deviations were also obtained when simulating the corresponding hydrocarbon (cyclopentane),[11] thus suggesting that the oxygen atom LJ parametrization or the electrostatic charge distribution is not the main reason for such a high deviation. Concerning tetrahydropyran, the average deviation on the vapor pressure (14%) is in better agreement than that of THF, as already observed for corresponding hydrocarbons (cyclohexane and cyclopentane). The vaporization enthalpy of tetrahydropyran is, however, slightly larger than that of cyclohexane (9% vs 4%).

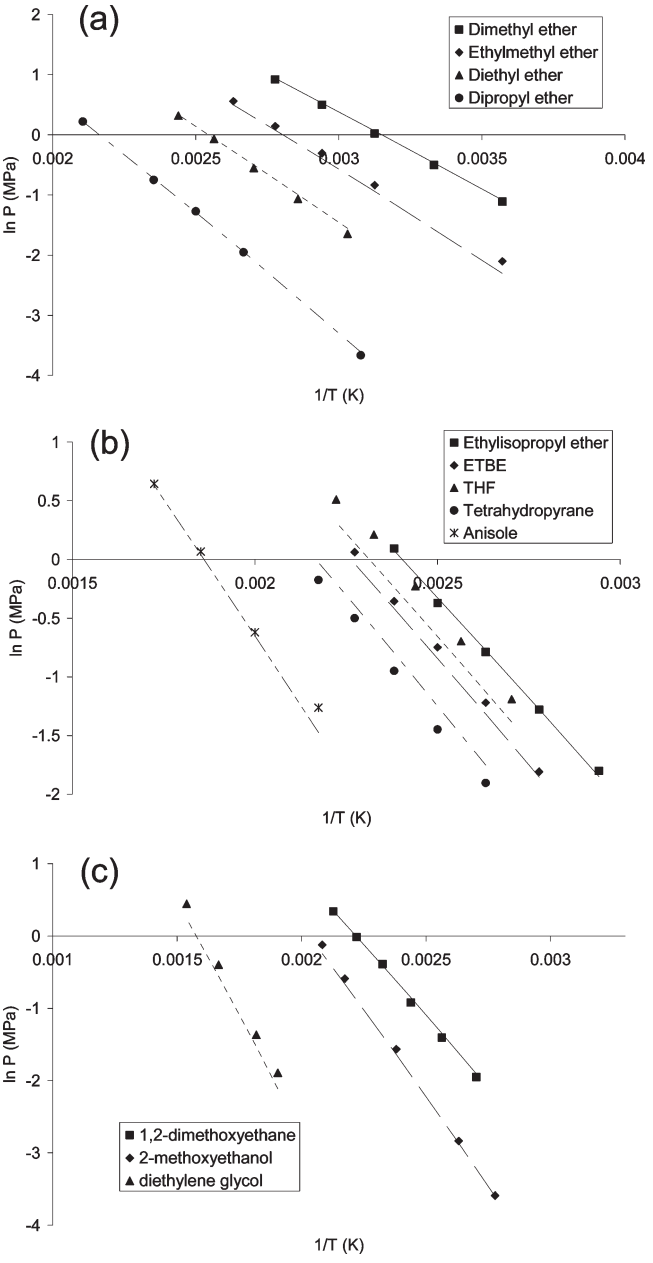

Figure 5. Experimental[15] (lines) and calculated (symbols) vapor pressures of linear ethers (a), branched, cyclic, and aromatic ethers (b), and multifunctional ethers (c).

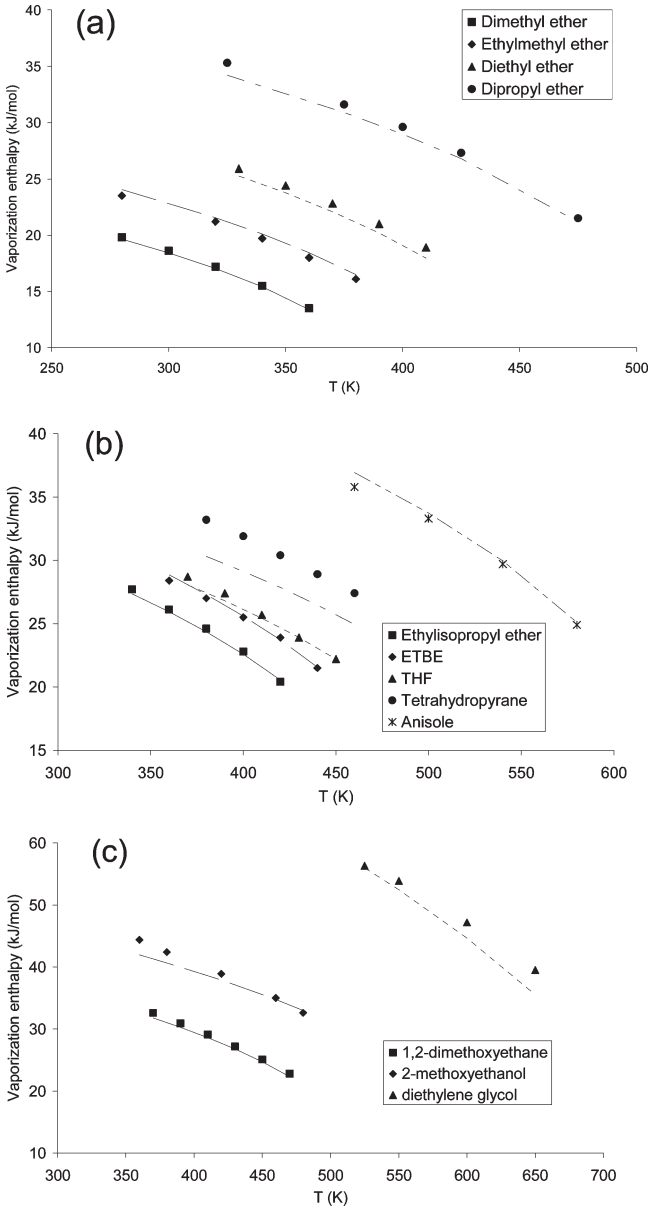

Figure 6. Experimental[15] (lines) and calculated (symbols) vaporization enthalpies of linear ethers (a), branched, cyclic, and aromatic ethers (b), and multifunctional ethers (c).

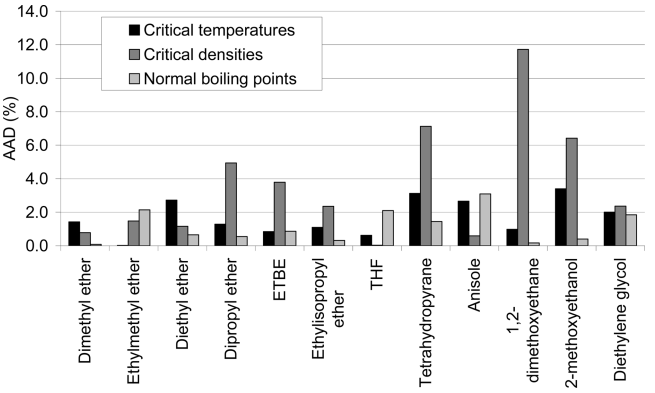

Figure 7. Average deviations between experimental[15] and calculated critical properties and normal boiling points. AAD(%) = abs($X^{calc} - X^{exp}$)/$X^{exp} \times 100$.

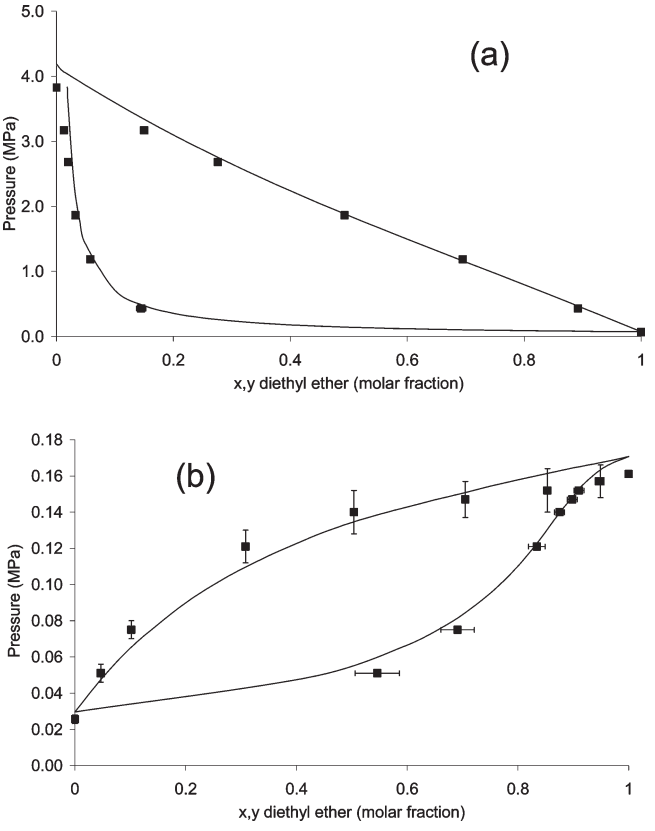

Figure 8. Experimental[44,45] (lines) and calculated (symbols) pressure−composition diagram of the diethyl ether + ethane mixture at 298.15 K (a) and diethyl ether + ethanol mixture at 323.15 K (b).

Concerning multifunctional ethers, a good agreement between experimental and calculated data is also observed since average deviations on saturated liquid densities, vapor pressures, and vaporization enthalpies are around 2%, 10%, and 3%, respectively. These results are particularly remarkable taking into account that no additional empirical parameters have been introduced to simulate such complex molecules, highlighting thus the transferability of the proposed force field. It can also be noticed that our new force field leads to a significant improvement in the pure compound vapor pressure prediction compared to the widespread TraPPE-UA force field, without altering the accuracy of the density prediction.

Finally, Figure 7 shows results obtained for critical properties and normal boiling point prediction. Numerical values are given in Supporting Information (Table S4). A good accuracy is reached since the average deviations between calculated and experimental are around 2%, 3.5%, and 1% for the critical temperatures, the critical densities, and the normal boiling points, respectively. The higher deviation is obtained for the critical density of 1,2-dimethoxyethane (11%). Nevertheless, experimental uncertainties reported in the literature[15] for this property are particularly high (25%).

The liquid phase structure of pure 2-methoxyethanol was also investigated at 298 K and 0.1 MPa. Intermolecular $O_{hydroxyl}-O_{hydroxyl}$ and $O_{ether}-O_{hydroxyl}$ radial distribution functions are given in the Supporting Information (Figure S3), and both

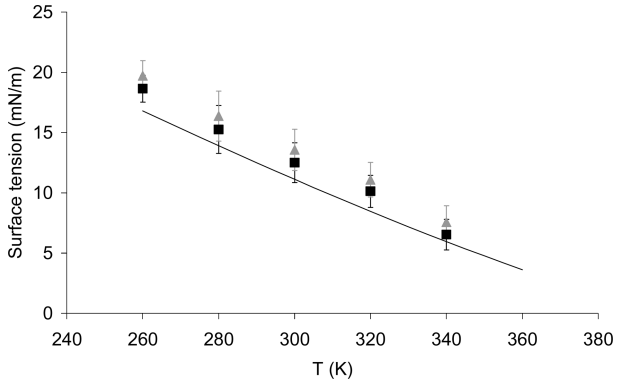

Figure 9. Surface tensions of the liquid−vapor interface of dimethyl ether. Solid line: experimental data,[46] squares: calculated with the IK method, triangles: calculated with the TA method.

Table 3. Experimental[46] (Smoothed) and Calculated (with IK and TA Methods) Liquid−Vapor Surface Tensions of Dimethyl Ether[a]

		γ_{IK} (mN/m)		γ_{TA} (mN/m)	
T (K)	γ_{exp} (mN/m)	total	LRC	total	LRC
260	17.35	18.6_{11}	3.2_1	19.7_{13}	2.2_1
280	14.40	15.3_{20}	2.9_1	16.4_{21}	2.1_1
300	11.55	12.5_{17}	2.5_1	13.6_{17}	1.8_1
320	8.81	10.1_{13}	2.1_1	11.1_{14}	1.5_1
340	6.18	6.53_{13}	1.5_1	7.55_{14}	1.3_1

[a] The subscripts give the accuracy of the last decimal, i.e., 18.6_{11} means 18.6 ± 1.1. The LRC columns give the contribution of the long range corrections to the total value of surface tension.

exhibit a peak located at 2.8 Å. At the intramolecular level, the $O_{ether}-H_{hydroxyl}$ histogram exhibits three peaks at 2.6, 3.9, and 4.3 Å corresponding to three stable conformations detailed in Figure S4 in the Supporting Information.

4.1.2. Binary Mixtures. Two binary mixtures are studied in this work: a polar + nonpolar system (diethyl ether + ethane at 298.15 K) and a polar + polar system (diethyl ether + ethanol at 323.15 K). In Figure 8 simulation results are compared to experimental data.[44,45] A good agreement between experiments and simulations is observed: deviations on bubble pressures are around 5 and 8%, respectively, while for the case of the vapor phase compositions, deviations are 15 and 6%, respectively. It is worth noticing that no modification of the force field has been carried out to simulate these mixtures: the same combining rules without introduction of empirical binary interaction parameters are employed. Such results emphasize thus the transferability of the developed force field to mixtures.

4.2. Liquid−Vapor Surface Tension. Experimental[46] and calculated liquid−vapor surface tensions of dimethyl ether are plotted in Figure 9, while numerical values are reported in Table 3. In this table are also reported the contributions of long-range corrections to the total surface tension values. Surface tensions and p_N-p_T profiles along the z-axis are given in the Supporting Information (Figure S6) as well as a snapshot of the liquid−vapor interface (Figure S5). Figure 10 shows coexistence densities ρ_{liq} and ρ_{vap} determined by fitting the equilibrium density profile to a hyperbolic tangent function of the

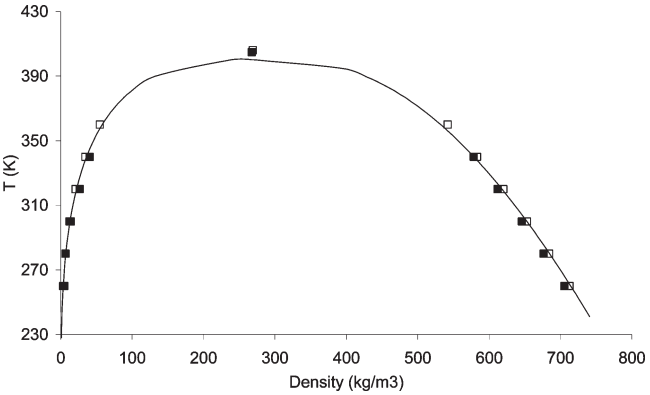

Figure 10. Vapor−liquid coexistence curve of dimethyl ether. Solid line: experimental data,[15,47] filled symbols: results from heterogeneous NVT simulations, open symbols: results from Gibbs ensemble simulations.

form:

$$\rho(z) = \frac{1}{2}(\rho_{liq} - \rho_{vap}) - \frac{1}{2}(\rho_{liq} - \rho_{vap})\tanh\left(\frac{2(z - z_0)}{d}\right) \quad (18)$$

where z_0 is the position of the Gibbs dividing surface and d an approximate measure of the interface thickness (adjustable parameters). An example of density profile along the z-axis is given in the Supporting Information (Figure S7). It can be seen in Figure 10 that the coexistence densities calculated from simulations in the heterogeneous NVT ensemble are consistent with those calculated in the Gibbs ensemble previously described. Both methods give similar deviations with experimental data for liquid densities (less than 1%). Simulations in the Gibbs ensemble indicate the model slightly overestimates this property as compared to experiment, whereas simulations in the heterogeneous NVT ensemble underestimate it. These small but systematic deviations observed between the two methods can be attributed to the explicit presence of the interface. The interface further attracts the ethers molecules and forms a small depletion zone in the liquid phase that may impact on the density of the liquid region close to the interface. It is indeed known[25] that two-phase systems with fewer than 1000 molecules are interface-dominated and that the two-phase simulations are rather designed to predict the interfacial properties.

For surface tension calculations, the statistical uncertainties range from 5% (at low reduced temperatures) to 20% (at high reduced temperatures), values sensibly larger than experimental uncertainties evaluated at 3%. The two calculation methods used (IK and TA) give similar results within statistical uncertainties. In the case of the IK method, the average deviation with experimental data is around 9%. It can be considered as an accurate prediction if we recall that the parameters of the interaction potential proposed in this work have not been optimized based on interfacial properties.

5. CONCLUSION

In this work, a new transferable force field has been proposed for ethers and glycol ethers. Only one new group has been

introduced, the ether oxygen atom, all of the other groups being directly taken from the AUA4 force field. The LJ parameters of this atom have been optimized based on the ethylmethyl ether saturated properties, and applied without further modifications to simulate a large variety of ethers: linear ethers (dimethyl ether, diethyl ether, dipropyl ether), branched ethers (ethylisopropyl ether, ETBE), cyclic ethers (THF, tetrahydropyrane), aromatic ether (anisole), diether (1,2-dimethoxyethane), and glycol ethers (2-methoxyethanol, diethylene glycol). For this purpose, three sets of partial electrostatic charges have been determined from quantum calculations according to the liquid phase dipole moment of the studied systems. Monte Carlo simulations performed with the new force field lead to accurate predictions of pure compound saturated properties, critical properties, liquid−vapor surface tensions, and pressure−composition binary mixture diagrams. The multifunctional molecules have been simulated using a recently proposed methodology for the calculation of the intramolecular electrostatic energy avoiding the use of additional empirical parameters. This new force field appears thus transferable to a wide variety of molecules and properties. It is furthermore worth noticing that binary mixtures have been simulated without introducing empirical binary parameters, highlighting in this way the transferability to mixtures. Hence, this new force field gives future opportunities to simulate complex systems of industrial interest involving molecules with ether functions.

■ ASSOCIATED CONTENT

Supporting Information. Tables and figures of additional information. Table S1 gives information about dipole moments of multifunctional ethers. Table S2 gives the Monte Carlo moves and attempts used during simulations. Table S3 reports experimental and calculated saturated properties, and Table S4 critical properties. In Figure S1 the experimental and predicted gas phase dipole moments of monofunctional ethers are plotted. Figure S2 describes the local dipoles in the studied multifunctional molecules. Figure S3 and S4 are related to radial distribution functions and stable conformations in 2-methoxyethanol. Figure S5 shows an example of configuration of the dimethyl ether liquid−vapor interface. Figure S6 gives surface tension profiles for dimethyl ether. Figure S7 gives an example of density profile for dimethyl ether. This material is available free of charge via the Internet at http://pubs.acs.org.

■ AUTHOR INFORMATION

Corresponding Author

*Tel.: +33 147526624. Fax: +33 147527025. E-mail: nicolas.ferrando@ifpen.fr.

■ ACKNOWLEDGMENT

A.D.M. acknowledges financial help from the Spanish Ministry of Science and Innovation MICINN via project CTQ2008-06469/PPQ.

■ REFERENCES

(1) Larsen, R.; Knight, C. A.; Sloan, E. D. *Fluid Phase Equilib.* **1998**, *150*, 353–360.
(2) Gavlin, G.; Goltsin, G. Gas Dehydration Process. U.S. Patent 5725637, Mar 10, 1998.
(3) Streicher, C. *Sulfur* **1997**, *250*, 60–64.
(4) Kowalewicz, A.; Wojtyniak, M. *Proc. Inst. Mech. Eng., Part D: J. Automobile Eng.* **2005**, *219* (D1), 103–125.
(5) Ramadhas, A. S.; Jayaraj, S.; Muraleedharan, C. *Int. J. Global Energies Issues* **2008**, *29*, 329–336.
(6) Ungerer, P.; Tavitian, B.; Boutin, A. *Applications of Molecular Simulation in the Oil and Gas Industry*, 1st ed.; Edition Technip: Rueil-Malmaison, France, 2005.
(7) Briggs, J. M.; Matsui, T.; Jorgensen, W. L. *J. Comput. Chem.* **1990**, *11* (8), 958–971.
(8) Stubbs, J. M.; Potoff, J. J.; Siepmann, J. I. *J. Phys. Chem. B* **2004**, *108* (45), 17596–17605.
(9) Ungerer, P.; Beauvais, C.; Delhommelle, J.; Boutin, A.; Rousseau, B.; Fuchs, A. H. *J. Chem. Phys.* **2000**, *112* (12), 5499–5510.
(10) Bourasseau, E.; Ungerer, P.; Boutin, A.; Fuchs, A. H. *Mol. Simul.* **2002**, *28* (4), 317–336.
(11) Bourasseau, E.; Ungerer, P.; Boutin, A. *J. Phys. Chem. B* **2002**, *106* (21), 5483–5491.
(12) Ahunbay, M. G.; Perez-Pellitero, J.; Contreras-Camacho, R. O.; Teuler, J. M.; Ungerer, P.; Mackie, A. D.; Lachet, V. *J. Phys. Chem. B* **2005**, *109* (7), 2970–2976.
(13) Ferrando, N.; Lachet, V.; Teuler, J. M.; Boutin, A. *J. Phys. Chem. B* **2009**, *113* (17), 5985–5995.
(14) Bourasseau, E.; Haboudou, M.; Boutin, A.; Fuchs, A. H.; Ungerer, P. *J. Chem. Phys.* **2003**, *118* (7), 3020–3034.
(15) DIPPR. *Data Compilation of Pure Compound Properties*; Taylor & Francis: London, 2010.
(16) Merker, T.; Engin, C.; Vrabec, J.; Hasse, H. *J. Chem. Phys.* **2010**, *132* (23), 234512.
(17) Eckl, B.; Vrabec, J.; Hasse, H. *J. Phys. Chem. B* **2008**, *112* (40), 12710–12721.
(18) Eckl, B.; Vrabec, J.; Hasse, H. *Mol. Phys.* **2008**, *106* (8), 1039–1046.
(19) Lide, D. R. *CRC Handbook of Chemistry and Physics*, 71st ed.; CRC Press: Boca Raton, FL, 1991.
(20) Cornell, W. D.; Cieplak, P.; Bayly, C. I.; Gould, I. R.; Merz, K. M.; Ferguson, D. M.; Spellmeyer, D. C.; Fox, T.; Caldwell, J. W.; Kollman, P. A. *J. Am. Chem. Soc.* **1995**, *117* (19), 5179–5197.
(21) Ungerer, P.; Lachet, V.; Tavitian, B. *Oil Gas Sci. Technol.* **2006**, *61* (3), 387–403.
(22) Panagiotopoulos, A. Z. *Mol. Phys.* **1987**, *61* (4), 813–826.
(23) Panagiotopoulos, A. Z. *Mol. Simul.* **1992**, *9* (1), 1–23.
(24) Allen, M. P.; Tildesley, D. J. *Computer Simulation of Liquids*; Oxford University Press: New York, 1987.
(25) Frenkel, D.; Smit, B. *Understanding Molecular Simulation: From Algorithms to Applications*; Academic Press: San Diego, 1996.
(26) Ferrando, N.; Lachet, V.; Boutin, A. *J. Phys. Chem. B* **2010**, *114* (26), 8680–8688.
(27) Ungerer, P.; Boutin, A.; Fuchs, A. H. *Mol. Phys.* **1999**, *97* (4), 523–539.
(28) Ungerer, P.; Boutin, A.; Fuchs, A. H. *Mol. Phys.* **2001**, *99* (17), 1423–1434.
(29) Ferrando, N.; Defiolle, D.; Lachet, V.; Boutin, A. *Fluid Phase Equilib.* **2010**, *299* (1), 132–140.
(30) Guo, M.; Lu, B. C. Y. *J. Chem. Phys.* **1997**, *106*, 473463.
(31) Goujon, F.; Malfreyt, P.; Boutin, A.; Fuchs, A. H. *J. Chem. Phys.* **2002**, *116* (18), 8106–8117.
(32) Irving, J. H.; Kirkwood, J. G. *J. Chem. Phys.* **1950**, *18*, 817–829.
(33) Gloor, G. J.; Jackson, G.; Blas, F. J.; de Miguel, E. *J. Chem. Phys.* **2005**, *123* (13), 134703.
(34) Biscay, F.; Ghoufi, A.; Goujon, F.; Lachet, V.; Malfreyt, P. *J. Phys. Chem. B* **2008**, *112* (44), 13885–13897.
(35) Biscay, F.; Ghoufi, A.; Goujon, F.; Lachet, V.; Malfreyt, P. *J. Chem. Phys.* **2009**, *130* (18), 184710.
(36) Biscay, F.; Ghoufi, A.; Lachet, V.; Malfreyt, P. *J. Chem. Phys.* **2009**, *131* (12), 124707.
(37) Trokhymchuk, A.; Alejandre, J. *J. Chem. Phys.* **1999**, *111* (18), 8510–8523.

(38) Goujon, F.; Malfreyt, P.; Simon, J. M.; Boutin, A.; Rousseau, B.; Fuchs, A. H. *J. Chem. Phys.* **2004**, *121* (24), 12559–12571.
(39) Ibergay, C.; Ghoufi, A.; Goujon, F.; Ungerer, P.; Boutin, A.; Rousseau, B.; Malfreyt, P. *Phys. Rev. E* **2007**, *75* (5), 051602.
(40) Orea, P.; Lopez-Lemus, J.; Alejandre, J. *J. Chem. Phys.* **2005**, *123* (11), 114702.
(41) Biscay, F.; Ghoufi, A.; Lachet, V.; Malfreyt, P. *J. Phys. Chem. B* **2009**, *113* (43), 14277–14290.
(42) Biscay, F.; Ghoufi, A.; Goujon, F.; Lachet, V.; Malfreyt, P. *J. Chem. Phys.* **2009**, *130* (18), 184710.
(43) Biscay, F.; Ghoufi, A.; Lachet, V.; Malfreyt, P. *Phys. Chem. Chem. Phys.* **2009**, *11* (29), 6132–6147.
(44) Ohgaki, K.; Sano, F.; Katayama, T. *J. Chem. Eng. Data* **1976**, *21* (1), 55–58.
(45) Nagai, J.; Ishii, N. *J. Soc. Chem. Ind. Jap.* **1935**, *38*, 86–95.
(46) Wu, J. T.; Liu, Z. G.; Wang, F. K.; Ren, C. *J. Chem. Eng. Data* **2003**, *48* (6), 1571–1573.
(47) *NIST TRC Thermo Table*, Version 2-2011-1-Pro; NIST: Gaithersburg, MD, 2011; http://wtt-pro.nist.gov/wtt-pro.